Origin of anomalous band-gap bowing in two-dimensional tin-lead mixed perovskite alloys

Qiang Gao,[1] Hasan Sahin,[2] Jun Kang,[1,*] and Su-Huai Wei[1]
[1]*Beijing Computational Science Research Center, Beijing 100193, China*
[2]*Department of Photonics, Izmir Institute of Technology, 35430 Izmir, Turkey*

(Received 1 February 2021; accepted 6 August 2021; published 20 August 2021)

The origin of the pronounced and composition-dependent band-gap bowing in Sn/Pb mixed perovskite alloys has been under debate for a long time. Previous studies reported conflicting results on whether the chemical or structural effect is the dominant mechanism. In this paper, the band-gap bowing effect and its possible origins in recently synthesized two-dimensional (2D) $Cs_2Pb_xSn_{1-x}I_2Cl_2$ alloys are investigated from first-principles calculations. In agreement with experiments, a large and composition-dependent bowing coefficient is observed. By analyzing the contribution from volume deformation, charge exchange, structural relaxation, and short-range order, it is found that the dominant mechanism causing the anomalous gap bowing is the structural relaxation-induced wave-function localization, forming isovalent-defect-like states, despite the negligible octahedral distortion and small lattice mismatch between the two end compounds. This is understood by the *s-p* repulsion-induced strong antibonding character of the valence-band maximum which leads to a large deformation potential, thus even a small atomic displacement can result in a large shift of the energy level. These results thus highlight the critical role of strong deformation potential and structural relaxation effect in unusual band evolution of 2D Sn/Pb perovskite alloys, and can be helpful to the modulation of their band gap for optoelectronic applications.

DOI: 10.1103/PhysRevB.104.064204

I. INTRODUCTION

Metal halide perovskites (MHPs) have emerged as promising candidates for photovoltaic and optoelectronic applications due to their high energy-conversion efficiency and relatively low cost [1–5]. Especially, compared to their three-dimensional (3D) bulk counterparts, two-dimensional (2D) layered MHPs exhibit much improved stability and a greater structural and chemical diversity, thus they have attracted an increasing amount of interest [6–9]. Various 2D MHPs, either hybrid organic-inorganic or all-inorganic, have been successfully synthesized, and their applications in high-efficiency solar cells [10,11], light-emitting diodes [12,13], and photodetectors [14,15] have been demonstrated. To optimize device performance, it is highly desirable to modulate the band gap of MHPs as needed. Such a demand has stimulated the need for considering alloys of different MHPs [16–18]. Among various types of MHP alloys, Sn/Pb mixed perovskite alloys are of particular interest. Different from the nearly linear change of band gap upon compositional variation in other types of halide alloys [19], pronounced nonlinear band-gap behaviors of both 3D, 2D, and one-dimensional Sn/Pb mixed perovskite alloys were reported [20–23]. Generally, the band gap of $A_{1-x}B_x$ semiconducting alloys can be expressed as [24]

$$E_g = (1-x)E_g(A) + xE_g(B) + bx(x-1), \qquad (1)$$

where b is defined as the bowing coefficient, measuring the deviation from the linear relationship (Vegard's law). The band-gap evolution in Sn/Pb perovskite alloys shows two anomalous features.

(I) The bowing coefficient is significant, and its value can be on the order of 1 eV, leading to a lower band gap than both end compounds [16,21].

(II) The bowing coefficient is not a constant, but strongly composition dependent [22,25].

Although the anomalous band-gap bowing in Sn/Pb perovskite alloys is well demonstrated both experimentally and theoretically, its origin is not fully understood, and several possible explanations were proposed in previous studies, mostly focused on the nonlayered 3D bulk cases. Im *et al.* [26] and Khatun *et al.* [25] proposed that the gap bowing is a combination of composition induced changes in spin-orbit coupling (SOC) and structural distortion. However, based on more detailed first-principles calculations, several works ruled out the contribution from SOC [20,27]. Eperon *et al.* suggested that short-range ordering of Sn/Pb atoms is the major origin of the bowing [27]. In contrast, Goyal *et al.* argued that the bowing is primarily a consequence of chemical mismatch between Sn and Pb, whereas the structural effect is negligible [20]. Valadares *et al.* also concluded that the arrangement of atomic orbitals is critical [28]. Dalpian *et al.* reported different results indicating that the large bowing should be related to structural changes, as they found the bowing parameters in intrinsic cubic phases are small [29]. Rajagopal *et al.* made similar conclusions that local structural relaxation (SR) effects are responsible for the anomalous bowing [30]. In short, previous studies provided conflicting mechanisms on the origin of the anomalous bowing in Sn/Pb perovskite alloys, and whether the gap bowing is a chemical effect or structural effect or both is still an open question.

Recently, all-inorganic Sn/Pb perovskite alloys $Cs_2Pb_xSn_{1-x}Cl_2I_2$ with 2D Ruddlesden-Popper (RP) phase have been synthesized [22], and the strong and

*jkang@csrc.ac.cn

composition-dependent gap bowing is also observed in this system. A major difference between 2D RP $Cs_2Pb_xSn_{1-x}Cl_2I_2$ and nonlayered 3D alloys like $MAPb_xSn_{1-x}X_3$ and $CsPb_xSn_{1-x}X_3$ is that the former has negligible octahedral distortion. The conflicting conclusions on the origin of the gap bowing made from those 3D alloys may partly be attributed to the sensitive dependence of octahedral distortion on the composition, which could strongly affect the band-gap values and thus bring much complexity into simulation (i.e., the magnitude of the distortion might be different with different computational methods). In the 2D case, considering the negligible octahedral distortion and small lattice mismatch (≈1%) between the end compounds $Cs_2PbI_2Cl_2$ and $Cs_2SnI_2Cl_2$, one can expect a small magnitude of structural relaxation in 2D $Cs_2Pb_xSn_{1-x}Cl_2I_2$ alloys. Therefore, the reduced complexity compared to the 3D case allows one to, in a systematic and controlled way, explore the contribution of chemical and structural effects to the anomalous bowing in 2D $Cs_2Pb_xSn_{1-x}Cl_2I_2$ alloys.

In this paper, the band-gap bowing effect and its possible origins in 2D $Cs_2Pb_xSn_{1-x}I_2Cl_2$ alloys are investigated from first-principles calculations. In agreement with experiments, strong composition dependence on the bowing coefficient is observed, especially in the dilute-Sn cases. The contributions from volume deformation (VD), charge exchange (CEX), structural relaxation, and short-range order (SRO) are analyzed. It is found that the main cause of anomalous bowing is structural relaxation, despite its small magnitude, and the contributions from other factors are minor. This is understood by the strong antibonding character of the valence-band maximum (VBM) state, which leads to a large deformation potential, thus a slight change in the bond length can induce a significant change of the valence-band offset and confinement of an isovalent-defect-like VBM state [24]. These results thus highlight the critical roles of strong deformation potential and structural relaxation effect in unusual band evolution of 2D Sn/Pb perovskite alloys, and can be helpful to the modulation of their band gap for optoelectronic applications.

II. METHODS

In this paper we consider 2D $Cs_2Pb_xSn_{1-x}Cl_2I_2$ alloys. All electronic structure calculations of 2D $Cs_2Pb_xSn_{1-x}Cl_2I_2$ alloys are based on the density functional theory (DFT) programmed in the Vienna *ab initio* simulation package (VASP) [31]. The core-valence interaction is approximated by the projector-augmented wave method [32]. The cutoff energy is selected as 300 eV. The exchange-correlation potential is described by the Perdew-Burke-Ernzerhof (PBE) functional of the generalized gradient approximation (GGA) formula [33]. SOC is included in the calculations of electronic structures. Calculations using the screened hybrid functional (HSE06) [34] with SOC are also carried out for the unit cell of 2D $Cs_2Pb(Sn)Cl_2I_2$, with a mixing parameter of 0.43. Except for the band-gap value, the band dispersions calculated by GGA-PBE and HSE06 are found to be similar, and both methods give type-II band alignment between the two materials. Therefore, the results for alloy calculations are obtained using GGA-PBE with SOC. The van der Waals interaction is treated by DFT-D3 method [35]. The convergence criteria of forces and energies are chosen to be 0.02 eV/Å and 10^{-4} eV during structure optimization and self-consistence calculations. An 8×8 supercell containing 448 atoms is constructed to study the properties of 2D $Cs_2Pb_xSn_{1-x}Cl_2I_2$ alloys, with a vacuum space of 20 Å. The Brillouin zone is sampled by the Γ point. It is worth mentioning that despite the 2D layered structure, the experimentally synthesized RP phase $Cs_2Pb_xSn_{1-x}I_2Cl_2$ remains a bulk material [22], which differs from the monolayer model we adopted here. Nevertheless, as discussed in the Supplemental Material [36], our analysis and tests indicate that the monolayer model is sufficiently accurate to describe the band bowing of bulk RP phase $Cs_2Pb_xSn_{1-x}I_2Cl_2$, and is computationally more efficient than the bulk model. Therefore, it is suitable to adopt the monolayer model. The "special quasi-random structure" (SQS) method [44,45] has been adopted to generate proper structures that can simulate alloys with random Sn/Pb distribution. We assume a linear relationship between the lattice constant of the alloy and the concentration, as confirmed by the experiment [22] and theoretical calculations [30]. To study the possibility of phase separation and the short-range-order effect, the cluster expansion (CE) model [46,47] is employed, as implemented in the ATAT code [48].

III. RESULTS AND DISCUSSION

To gain a whole perspective on the electronic properties of 2D $Cs_2Pb_xSn_{1-x}I_2Cl_2$ alloys, we first discuss the structural and electronic properties of the two constituents (monolayer $Cs_2PbI_2Cl_2$ and $Cs_2SnI_2Cl_2$). As seen in Figs. 1(a) and 1(b), monolayer $Cs_2PbI_2Cl_2$ and $Cs_2SnI_2Cl_2$ can be viewed as 2D octahedron planes. The Sn/Pb ions occupy the center of the octahedron. The Cl ions take the in-plane sites and serve as shared corners of the octahedron, whereas the I ions locate at the out-of-plane sites. The Cs ions provide extra electrons to ensure charge balance. The optimized lattice constants for monolayer $Cs_2PbI_2Cl_2$ and $Cs_2SnI_2Cl_2$ are 5.71 and 5.65 Å, respectively, which agree well with the values in previous works [49,50]. Experimentally, it is reported that unlike nonlayered 3D perovskites $APb(Sn)X_3$, there is no octahedral distortion or tilting in 2D $Cs_2PbI_2Cl_2$ and $Cs_2SnI_2Cl_2$ [22]. Our phonon spectrum calculations further support this conclusion as no negative frequency is observed for the undistorted systems (see Fig. S1 in the Supplemental Material [36]), also in agreement with Acharyya *et al.*'s calculations [51]. The electronic structures of monolayer $Cs_2Pb(Sn)I_2Cl_2$ were calculated in Fig. 1(c). Both monolayer $Cs_2PbI_2Cl_2$ and $Cs_2SnI_2Cl_2$ possess direct band structures with band-gap values of 1.68 and 1.39 eV calculated by PBE-SOC. We also performed test calculations using HSE-SOC and found similar band dispersions with larger band gaps (2.91 eV for $Cs_2PbI_2Cl_2$ and 2.50 eV for $Cs_2SnI_2Cl_2$) (see Fig. S2 in the Supplemental Material [36]). The two constituents form a type-II band alignment [Fig. 1(d)], and the offset in the valence band (0.63 eV for PBE-SOC and 0.84 eV for HSE-SOC) is much larger than that in the conduction band (0.34 eV for PBE-SOC and 0.43 eV for HSE-SOC). Since PBE-SOC and HSE-SOC give similar band dispersion and the same type-II band alignment (the same trends) between the two materials, it is reasonable to use PBE-SOC to describe the trends in the band gap of their alloys. Similar to other Sn- or Pb-based

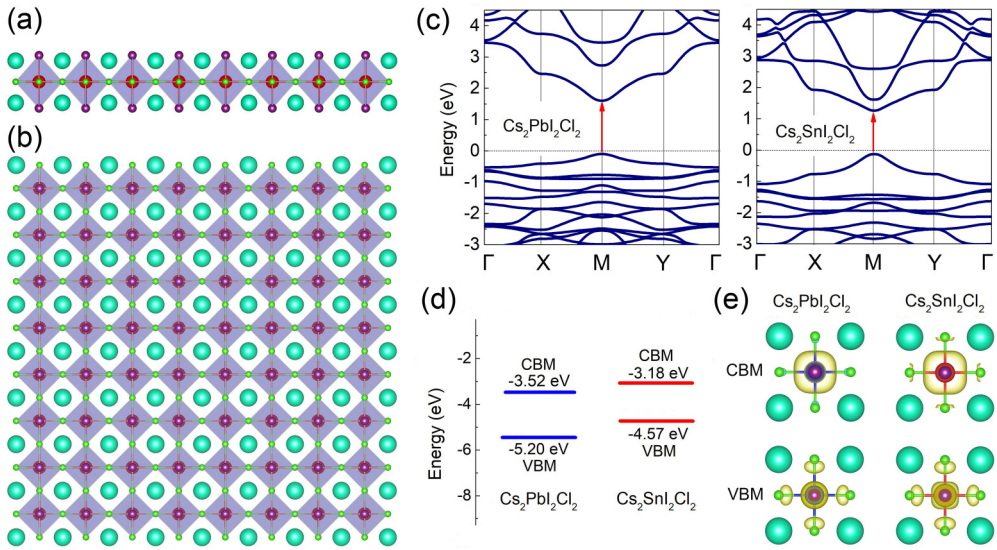

FIG. 1. Structures for side (a) and top (b) view, band structures (c), band alignment relative to the vacuum level of monolayer $Cs_2Pb(Sn)I_2Cl_2$ (d), and the charge densities of CBM and VBM (wave function norm square) (e). Cyan, green, purple, blue, and red balls representing Cs, Cl, I, Pb, and Sn atoms, respectively.

halide perovskites [52–55], the conduction-band minimum (CBM) of $Cs_2Pb(Sn)I_2Cl_2$ mainly consists of Pb/Sn p states, whereas the VBM originates from the antibonding interaction between Pb/Sn s states and I/Cl p states [Fig. 1(e)].

Next, we study the band bowing effect in 2D $Cs_2Pb_xSn_{1-x}I_2Cl_2$ alloys. We first consider fully mixed alloys with random Sn/Pb distribution, and the corresponding structures were generated using the SQS approach with an 8×8 supercell. Note we keep the ordered Cl/I arrangement in the alloys since random distribution of Cl/I is energetically not favored according to our test calculations (see Sec. VI in the Supplemental Material [36]), and not observed in previous experiments [22]. This can be attributed to the large strain energy caused by atomic size mismatch in the Cl/I disordered structures. In Fig. 2(a), the band-gap value of the alloys with different Pb concentration x is plotted. The calculations well reproduce the trends observed in experimental synthesized 2D RP phase $Cs_2Pb_xSn_{1-x}I_2Cl_2$ alloys [22]. In contrast to many conventional semiconductors exhibiting a constant bowing parameter, the band gap versus x relationship of 2D $Cs_2Pb_xSn_{1-x}I_2Cl_2$ alloys can be divided into two regions. When x is larger than 0.75, the band gap decreases rapidly as x decreases with a large and composition-dependent bowing parameter (which can exceed 4 eV). When x is less than 0.75, the gap bowing becomes much less significant, with an almost constant bowing parameter around 0.5 eV. Numeric fitting on the x-dependent band bowing parameter and band gap is provided in Sec. III of the Supplemental Material [36]. To explore whether the CBM or VBM contributes to the large bowing when x is close to 1, the positions of the CBM and VBM with respect to the vacuum level are plotted in Fig. 2(b) as a function of x. It is seen that the CBM always exhibits a small bowing. In contrast, the bowing of the VBM is concentration dependent. When x is less than 0.75, the VBM bowing is weak. Once x exceeds 0.75, the VBM bowing is greatly enhanced. Therefore, the strong band-gap bowing of 2D $Cs_2Pb_xSn_{1-x}I_2Cl_2$ alloys at large x is dominated by the VBM.

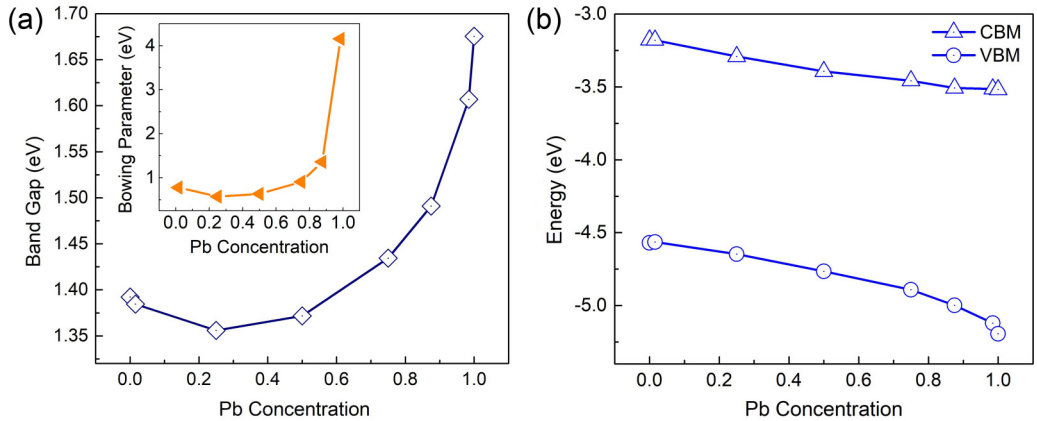

FIG. 2. Band gap and bowing parameters (a) and band edge energy (b) of 2D $Cs_2Pb_xSn_{1-x}I_2Cl_2$ alloys as functions of Pb concentration. Band edge energy is aligned relative to the vacuum level.

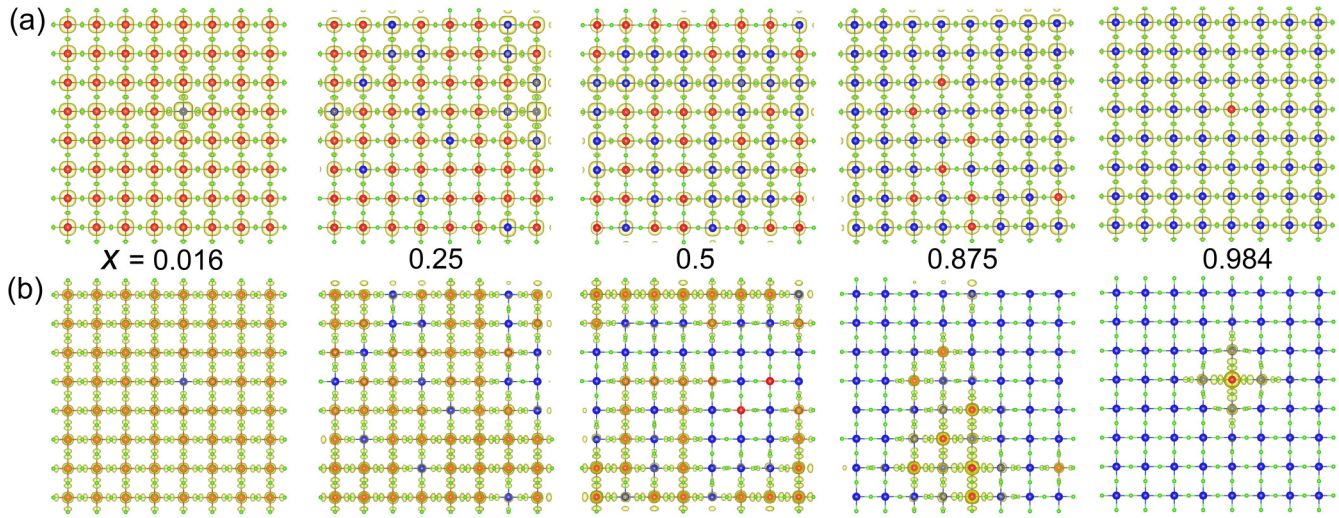

FIG. 3. The charge densities of CBM (a) and VBM (b) of 2D $Cs_2Pb_xSn_{1-x}I_2Cl_2$ alloys for different Pb concentrations (x); Cs and I atoms are omitted to show the distribution of Sn and Pb atoms more clearly.

To further study the nature of the band bowing, the charge densities of CBM and VBM of 2D $Cs_2Pb_xSn_{1-x}I_2Cl_2$ alloys for different concentration are plotted in Fig. 3. For the CBM, the wave functions are delocalized and mainly originate from Pb/Sn atoms. Moreover, the spatial distribution of these delocalized states shows weak dependence on Pb concentration. Thus, the CBM always exhibits a bandlike behavior, consistent with its small bowing effect in Fig. 2(b). For the VBM, the wave functions are also quite delocalized and bandlike when Pb concentration is less than 0.75. However, in the dilute-Sn limit ($x = 0.984$), the distribution of the VBM is highly localized at the Sn site, much like a "deep" impurity state. Such isovalent-impurity-like behavior persists at the region $x > 0.75$, even with a considerable Sn concentration. In this case, the composition dependence of the impurity gap cannot be described by a constant b in Eq. (1) which describes a bandlike behavior [24]. As a result, a large and nonconstant bowing is observed.

In order to understand the physical origins of the composition-dependent bowing and the impurity-like VBM, one can decompose the formation of 2D $Cs_2Pb_xSn_{1-x}I_2Cl_2$ alloys into three steps [47]: (i) VD—deform the equilibrium cell volume and the bond length of the constituents to the corresponding concentration averaged values; (ii) CEX—mix the two types of cations (Sn and Pb) into the lattice of an unrelaxed alloy supercell constructed from the deformed unit cell in (i); and (iii) SR—fully relax the alloy structure. The bowing parameter can thus be expressed by the contributions from different steps (see the Supplemental Material for a detailed explanation [36]):

$$b = b_{\mathrm{VD}} + b_{\mathrm{CE}} + b_{\mathrm{SR}}. \tag{2}$$

As mentioned in the introduction, for bulk Sn/Pb alloy perovskites, there have been several studies investigating which process dominates their strong band-gap bowing. On the one hand, composition-induced changes of the crystal structure (VD+SR) are predicted due to the octahedral distortion [26,30]. On the other hand, there is also chemical difference and energy mismatch between Sn and Pb, thus results in CEX [20,28]. However, whether the band-gap bowing mainly originates from the CEX process or the VD+SR process is still under debate. In contrast to the nonlayered bulk case, there is negligible octahedral distortion in 2D $Cs_2Pb_xSn_{1-x}I_2Cl_2$ alloys as confirmed by experiment and our phonon calculation (Fig. S1 [36]). Thus, the main consequence of the VD+SR process is bond length change in the alloys. Since the VBM has anion p and cation s characters, the wave-function localization can be related to the s-p coupling. The type-II band alignment in Fig. 1(d) between $CsSnI_2Cl_2$ and $CsPbI_2Cl_2$ indicates stronger s-p coupling in the former, which thus creates a potential well with depth of ΔV for holes in the alloys, and a deeper well leads to stronger localization. On the one hand, the s-p coupling strength is affected by the energy separation between anion p orbital and cation s orbital. Compared to the 5s orbital of Pb, the 4s orbital of Sn is closer to the anion p orbital, and ΔV will be larger if the energy difference between Sn 4s and Pb 5s is larger. On the other hand, a smaller bond length between anion and cation can also lead to stronger s-p coupling and larger ΔV. Therefore, the depth ΔV of the s-p coupling induced potential well depends on both chemical and structural effects. Considering the small lattice mismatch (≈1%) between monolayer $Cs_2PbI_2Cl_2$ and $Cs_2SnI_2Cl_2$, one would expect weak structural effects in the alloys, and thus the domination of chemical effect to the band bowing. In Fig. 4(a), the decomposed bowing parameters b_{VD}, b_{CE} and b_{SR} for different composition x are presented. The b_{VD} is negligible as expected. However, contrary to the above prediction, it is seen that b_{CE} only shows weak composition dependence. The nonlinear behavior is much more significant for b_{SR}, the value of which is larger than b_{CE} for all x, especially in the impuritylike region (x close to 1). Therefore, structural relaxation is the major cause of the large and strongly composition-dependent gap bowing in 2D $Cs_2Pb_xSn_{1-x}I_2Cl_2$ alloys. This is further supported by the VBM charge densities of the unrelaxed and relaxed structures at the dilute-Sn limit. As seen in Figs. 4(c) and 4(d), in the unrelaxed structure, the CEX only results in weak localization of the VBM, exhibiting a shallow-impurity-like character. With

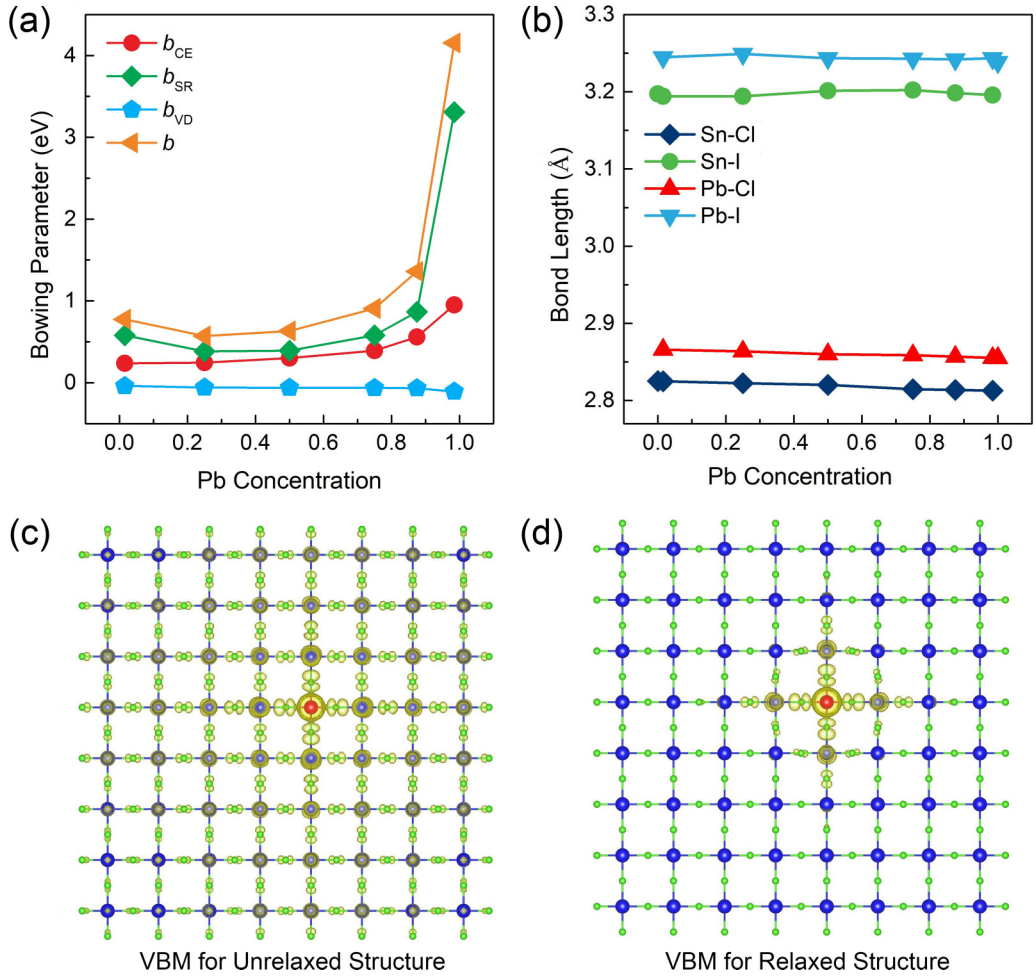

FIG. 4. Band gap bowing parameters (a) and bond length (b) of 2D $Cs_2Pb_xSn_{1-x}I_2Cl_2$ alloys as functions of Pb concentration. (c), (d) The charge densities of VBM of 2D $Cs_2Pb_xSn_{1-x}I_2Cl_2$ alloys for unrelaxed and relaxed structure at Pb concentration = 0.984.

structural relaxation, the localization is much enhanced and deep-impurity-like character is observed.

To gain a deeper insight into the significant SR term, we calculated the averaged bond length in relaxed alloy structure at different concentration, as shown in Fig. 4(b). It is observed that the Sn-X and Pb-X bond lengths (X = I, Cl) in the alloys show a bimodal distribution. The extent of relaxation can be described by the bond length relaxation parameters [56]:

$$\varepsilon = (R_{\mathrm{Pb}-X} - R_{\mathrm{Sn}-X})/\left(R^0_{\mathrm{Pb}-X} - R^0_{\mathrm{Sn}-X}\right), \tag{3}$$

where R and R^0 are the bond lengths in the alloys and the pure constitutions, respectively. $\varepsilon = 0$ corresponds to no relaxation, while $\varepsilon = 1$ means full relaxation. We found that ε is always close to 1 for 2D $Cs_2Pb_xSn_{1-x}I_2Cl_2$ alloys, indicating that a full relaxation occurs in this ionic system, and the bond lengths in the alloys are almost the same as those in the pure constitutions. Because the VBM of the alloys has strong antibonding character, it can have large deformation potential, thus its position can be sensitive to the change in bond length, even if such change is not large. In the fully relaxed dilute-Sn alloys, the Sn-X bond lengths are ≈1% (about 0.03 Å) smaller than those in the unrelaxed structure. We have calculated the VBM energy of monolayer $CsSnI_2Cl_2$ with its atomic coordination fixed at that of $CsPbI_2Cl_2$, and compared with the case of fully relaxed $CsSnI_2Cl_2$. It is found that ≈1% bond length reduction in $Cs_2SnI_2Cl_2$ can already push up its VBM state by 0.2 eV, which corresponds to a large deformation potential of ≈20 eV. Hence, the s-p coupling induced potential well becomes much deeper when full relaxation occurs, and the VBM state becomes much more localized. Therefore, the significant SR effect can be attributed to the antibonding character and the large deformation potential of the VBM. Moreover, for hybrid RP Sn/Pb perovskite alloys, the octahedral distortion caused by the organic spacer may further enhance the SR effect (more discussions are provided in Sec. V in the Supplemental Material [36]).

In the above discussion we assumed fully mixed 2D $Cs_2Pb_xSn_{1-x}I_2Cl_2$ alloys with random distribution of Pb and Sn atoms. Nevertheless, phase separation or SRO can often occur in alloys, which could change the electronic properties as compared with the case of random alloys. For nonlayered bulk Sn/Pb alloy perovskites, it has been proposed that the ordering of Pb and Sn atoms into clusters contributes to the band-gap bowing [27]. For 2D $Cs_2Pb_xSn_{1-x}I_2Cl_2$ alloys studied here, if clustering of Sn occurs, effectively the width of the s-p coupling induced potential well increases. This could enhance the localization of VBM and contribute to

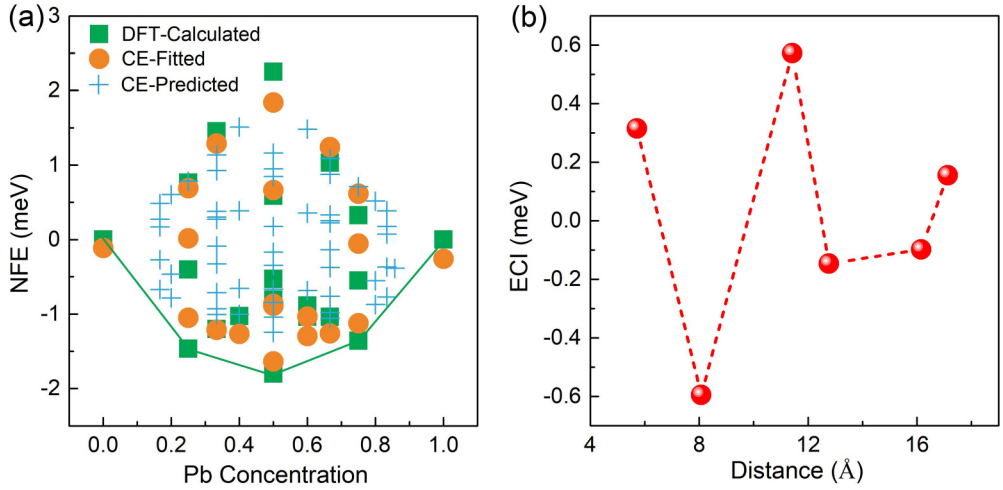

FIG. 5. (a) Normalized formation energy (NFE) of 2D $Cs_2Pb_xSn_{1-x}I_2Cl_2$ alloys for different Pb concentrations. (b) Fitted ECIs for pairs from the nearest to the sixth neighbors.

the band-gap bowing. Therefore, in the following we discuss the possible effect of SRO in 2D $Cs_2Pb_xSn_{1-x}I_2Cl_2$ alloys on the band-gap bowing. For this purpose, we construct a CE model [46,47] to describe the formation energy of 2D $Cs_2Pb_xSn_{1-x}I_2Cl_2$ alloy structure with configuration σ, namely,

$$E(\sigma) = \sum_i m_i J_i \bar{\Pi}_i(\sigma) \tag{4}$$

Here $E(\sigma)$ is the formation energy per Sn/Pb site of the alloys. i denotes a cluster (pairs, triplets, quadruplets, etc.), and m_i is the multiplicity of symmetry-equivalent clusters. J_i is the effective cluster interaction (ECI) for i, and $\bar{\Pi}_i(\sigma)$ is the average of the atomic correlation functions of cluster i. In the current paper, the clusters included are zero, onsite, and pairs up to the sixth neighbors. In Fig. 5(a) the DFT calculated and CE fitted formation energies of the alloys are shown. It is interesting to note that for many configurations, the formation energy can be negative. Three stable ground states (under 0 K) with periodic structures at $x = 0.25$, 0.5, and 0.75 were predicted and the corresponding configurations were shown in the Supplemental Material [36]. The negative formation energy can be understood by the Coulomb energy gain due to charge redistribution in strongly ionic alloys [19]. The fitted ECIs for pairs from the nearest to the sixth neighbors are shown in Fig. 5(b). The ECI of the nearest-neighbor pair is positive, which results in repulsion between atoms with the same species and prevents phase separation. It is also noted that the magnitude of the ECIs is less than 1 meV, much smaller than that in highly ordered perovskite alloys (e.g., 10–100 meV in $Cs_2AgBiBr_6$ [57]). This suggests weak SRO in $Cs_2Pb_xSn_{1-x}I_2Cl_2$. Based on the cluster expansion Hamiltonian [Eq. (4)] and the calculated ECIs, Monte Carlo simulations were performed using a 10×10 supercell for different concentration x, and the statistical averages of the atomic correlation functions for pairs up to the sixth neighbor are computed to explore possible SRO. It is found that at 300 K, the averaged atomic correlation functions (thus the atomic configuration) are very close to those in random alloys, and the difference is within 0.032, which is comparable to the tolerance in generating the SQS structure. In reality, the deviation could be even smaller considering that the experimental growth temperature of 2D $Cs_2Pb_xSn_{1-x}I_2Cl_2$ alloys is 800 K [22]. Therefore, the effect of SRO on the composition-dependent band-gap bowing is minor.

IV. CONCLUSIONS

In summary, the band-gap bowing effect and its possible origins in 2D $Cs_2Pb_xSn_{1-x}I_2Cl_2$ alloys are investigated from first-principles calculations. Two regions were observed in the band-gap variation as a function of x: (i) a bandlike region ($x < 0.75$) where the band edge states are delocalized, with a small (<1eV) and nearly constant bowing coefficient, and (ii) an impuritylike region ($x > 0.75$) where the VBM state is strongly localized, with a large (up to 4 eV) and composition-dependent bowing coefficient. By analyzing the contribution from volume deformation, charge exchange, and structural relaxation, it is found that the dominant mechanism causing the large and strongly composition-dependent gap bowing is the structural relaxation process, despite the small lattice mismatch between the two constitutes. This is understood by the antibonding character of the VBM which leads to a large deformation potential, thus even a small atomic displacement can result in a large shift of the energy level. With cluster expansion calculations, it is also demonstrated that there is no phase separation in the alloys, and SRO is negligible due to the weak ECIs. Overall, structural relaxation is the main reason for the large and nonconstant band-gap bowing coefficient in 2D $Cs_2Pb_xSn_{1-x}I_2Cl_2$ alloys. These results thus highlight the critical role of strong deformation potential and structural relaxation effect in unusual band evolution of 2D Sn/Pb perovskite alloys, and can be helpful to the modulation of their band gap for optoelectronic applications.

ACKNOWLEDGMENTS

This work was supported by NSFC (Grants No. 12074029, No. 11991060, No. 11634003, No. 12088101, and No.

U1930402) and the Key Research and Development Program of Beijing (Grant No. Z181100005118003). Computational resources were provided by Tianhe2-JK at Beijing Computational Science Research Center.

[1] J. S. Manser, J. A. Christians, and P. V. Kamat, Chem. Rev. **116**, 12956 (2016).
[2] A. Mei, X. Li, L. Liu, Z. Ku, T. Liu, Y. Rong, M. Xu, M. Hu, J. Chen, Y. Yang, M. Grätzel, and H. Han, Science **345**, 295 (2014).
[3] J. H. Heo, H. J. Han, D. Kim, T. K. Ahn, and S. H. Im, Energy Environ. Sci. **8**, 1602 (2015).
[4] M. M. Lee, J. Teuscher, T. Miyasaka, T. N. Murakami, and H. J. Snaith, Science **338**, 643 (2012).
[5] M. Yuan, L. N. Quan, R. Comin, G. Walters, R. Sabatini, O. Voznyy, S. Hoogland, Y. Zhao, E. M. Beauregard, P. Kanjanaboos, Z. Lu, D. H. Kim, and E. H. Sargent, Nat. Nanotechnol. **11**, 872 (2016).
[6] E. Shi, Y. Gao, B. P. Finkenauer, A. H. Coffey Akriti, and L. Dou, Chem. Soc. Rev. **47**, 6046 (2018).
[7] L. Dou, A. B. Wong, Y. Yu, M. Lai, N. Kornienko, S. W. Eaton, A. Fu, C. G. Bischak, J. Ma, T. Ding, N. S. Ginsberg, L.-W. Wang, A. P. Alivisatos, and P. Yang, Science **349**, 1518 (2015).
[8] J. W. Lee, Z. Dai, T. H. Han, C. Choi, S. Y. Chang, S. J. Lee, N. D. Marco, H. Zhao, P. Sun, Y. Huang, and Y. Yang, Nat. Commun. **9**, 3021 (2018).
[9] C. C. Stoumpos, D. H. Cao, D. J. Clark, J. Young, J. M. Rondinelli, J. I. Jang, J. T. Hupp, and M. G. Kanatzidis, Chem. Mater. **28**, 2852 (2016).
[10] H. Tsai, W. Nie, J. C. Blancon, C. C. Stoumpos, R. Asadpour, B. Harutyunyan, A. J. Neukirch, R. Verduzco, J. J. Crochet, S. Tretiak, L. Pedesseau, J. Even, M. A. Alam, G. Gupta, J. Lou, P. M. Ajayan, M. J. Bedzyk, M. G. Kanatzidis, and A. D. Mohite, Nature (London) **536**, 312 (2016).
[11] I. C. Smith, E. T. Hoke, D. Solis-Ibarra, M. D. McGehee, and H. I. Karunadasa, Angew. Chem. Int. Ed. **53**, 11232 (2014).
[12] N. Wang, L. Cheng, R. Ge, S. Zhang, Y. Miao, W. Zou, C. Yi, Y. Sun, Y. Cao, R. Yang, Y. Wei, Q. Guo, Y. Ke, M. Yu, Y. Jin, Y. Liu, D. Di Q.Ding, L. Yang, G. Xing, H. Tian, C. Jin, F. Gao, R. H. Friend, J. Wang, and W. Huang, Nat. Photon. **10**, 699 (2016).
[13] H. Tsai, C. Liu, E. Kinigstein, M. Li, S. Tretiak, M. Cotlet, X. Ma, X. Zhang, and W. Nie, Adv. Sci. **7**, 1903202 (2020).
[14] J. Song, L. Xu, J. Li, J. Xue, Y. Dong, X. Li, and H. Zeng, Adv. Mater. **28**, 4861 (2016).
[15] Y. Liu, H. Ye, Y. Zhang, K. Zhao, Z. Yang, Y. Yuan, H. Wu, G. Zhao, Z. Yang, J. Tang, Z. Xu, and S. Liu, Matter **1**, 465 (2019).
[16] F. Hao, C. C. Stoumpos, R. P. H. Chang, and M. G. Kanatzidis, J. Am. Chem. Soc. **136**, 8094 (2014).
[17] Y. Ogomi, A. Morita, S. Tsukamoto, T. Saitho, N. Fujikawa, Q. Shen, T. Toyoda, K. Yoshino, S. S. Pandey, T. Ma, and S. Hayase, J. Phys. Chem. Lett. **5**, 1004 (2014).
[18] L. Protesescu, S. Yakunin, M. I. Bodnarchuk, F. Krieg, R. Caputo, C. H. Hendon, R. X. Yang, A. Walsh, and M. V. Kovalenko, Nano Lett. **15**, 3692 (2015).
[19] W. J. Yin, Y. Yan, and S. H. Wei, J. Phys. Chem. Lett. **5**, 3625 (2014).
[20] A. Goyal, S. McKechnie, D. Pashov, W. Tumas, M. van Schilfgaarde, and V. Stevanović, Chem. Mater. **30**, 3920 (2018).
[21] Y. Zong, N. Wang, L. Zhang, M. G. Ju, X. C. Zeng, X. W. Sun, Y. Zhou, and N. P. Padture, Angew. Chem. Int. Ed. **56**, 12658 (2017).
[22] J. Li, Q. Yu, Y. He, C. C. Stoumpos, G. Niu, G. G. Trimarchi, H. Guo, G. Dong, D. Wang, L. Wang, and M. G. Kanatzidis, J. Am. Chem. Soc. **140**, 11085 (2018).
[23] T. Lei, M. Lai, Q. Kong, D. Lu, W. Lee, L. Dou, V. Wu, Y. Yu, and P. Yang, Nano Lett. **18**, 3538 (2018).
[24] S. H. Wei and A. Zunger, Phys. Rev. Lett. **76**, 664 (1996).
[25] S. Khatun, A. Maiti, and A. J. Pal, Appl. Phys. Lett. **116**, 012104 (2020).
[26] J. Im, C. C. Stoumpos, H. Jin, A. J. Freeman, and M. G. Kanatzidis, J. Phys. Chem. Lett. **6**, 3503 (2015).
[27] G. E. Eperon, T. Leijtens, K. A. Bush, R. Prasanna, T. Green, J. T. W. Wang, D. P. McMeekin, G. Volonakis, R. L. Milot, R. May, A. Palmstrom, D. J. Slotcavage, R. A. Belisle, J. B. Patel, E. S. Parrott, R. J. Sutton, W. Ma, F. Moghadam, B. Conings, A. Babayigit, H. Boyen, S. Bent, F. Giustino, L. M. Herz, M. B. Johnston, M. D. McGehee, and H. J. Snaith, Science **354**, 861 (2016).
[28] F. Valadares, I. Guilhon, L. K. Teles, and M. Marques, J. Phys. Chem. C **124**, 26124 (2020).
[29] G. M. Dalpian, X. G. Zhao, L. Kazmerski, and A. Zunger, Chem. Mater. **31**, 2497 (2019).
[30] A. Rajagopal, R. J. Stoddard, H. W. Hillhouse, and A. K. Y. Jen, J. Mater. Chem. A **7**, 16285 (2019).
[31] G. Kresse and J. Furthmüller, Phys. Rev. B **54**, 11169 (1996).
[32] P. E. Blöchl, Phys. Rev. B **50**, 17953 (1994).
[33] J. P. Perdew, K. Burke, and M. Ernzerhof, Phys. Rev. Lett. **77**, 3865 (1996).
[34] J. Heyd, J. E. Peralta, G. E. Scuseria, and R. L. Martin, J. Chem. Phys. **123**, 174101 (2005).
[35] S. Grimme, J. Antony, S. Ehrlich, and H. Krieg, J. Chem. Phys. **132**, 154104 (2010).
[36] See Supplemental Material at http://link.aps.org/supplemental/10.1103/PhysRevB.104.064204 for the results of the phonon spectra and HSE-SOC band structures of monolayer $Cs_2Pb(Sn)I_2Cl_2$; numeric fitting of the bowing coefficient and band gap; calculation details on the decomposition of bowing parameters; possible effects of organic spacers in RP Sn/Pb perovskite alloys; discussions on anion disorder; the rationality of the monolayer model; stable ground states of monolayer $Cs_2Pb_xSn_{1-x}I_2Cl_2$ alloys; and CIF-format structure files of constructed alloy supercells. References [14,22,37–43] are included in the Supplemental Material.
[37] J. E. Bernard and A. Zunger, Phys. Rev. B **36**, 3199 (1987).
[38] M. Ferhat and F. Bechstedt, Phys. Rev. B **65**, 075213 (2002).
[39] J. Li, C. C. Stoumpos, G. G. Trimarchi, I. Chung, L. Mao, M. Chen, M. R. Wasielewski, L. Wang, and M. G. Kanatzidis, Chem. Mater. **30**, 4847 (2018).

[40] H. Lu, C. Xiao, R. Song, T. Li, A. E. Maughan, A. Levin, R. Brunecky, J. J. Berry, D. B. Mitzi, V. Blum, and M. C. Beard, J. Am. Chem. Soc. **142**, 13030 (2020).
[41] J. Yin, P. Maity, R. Naphade, B. Cheng, J. He, O. M. Bakr, J. Bredas, and O. F. Mohammed, ACS Nano **13**, 12621 (2019).
[42] Y. Yu, D. Zhang, and P. Yang, Nano Lett. **17**, 5489 (2017).
[43] Q. A. Akkerman, E. Bladt, U. Petralanda, Z. Dang, E. Sartori, D. Baranov, A. L. Abdelhady, I. Infante, S. Bals, and L. Manna, Chem. Mater. **31**, 2182 (2019).
[44] A. Zunger, S. H. Wei, L. G. Ferreira, and J. E. Bernard, Phys. Rev. Lett. **65**, 353 (1990).
[45] S. H. Wei, L. G. Ferreira, J. E. Bernard, and A. Zunger, Phys. Rev. B **42**, 9622 (1990).
[46] J. M. Sanchez, F. Ducastelle, and D. Gratias, Physica A **128**, 334 (1984).
[47] L. G. Ferreira, S. H. Wei, and A. Zunger, Phys. Rev. B **40**, 3197 (1989).
[48] A. van de Walle, M. Asta, and G. Ceder, Calphad **26**, 539 (2002).
[49] Z. Xu, M. Chen, and S. Liu, J. Phys. Chem. C **123**, 27978 (2019).
[50] Z. Li, X. Liu, J. Xu, S. Yang, H. Zhao, H. Huang, S. F. Liu, and J. Yao, J. Phys. Chem. Lett. **11**, 4138 (2020).
[51] P. Acharyya, T. Ghosh, K. Pal, K. Kundu, K. S. Rana, J. Pandey, A. Soni, U. V. Waghmare, and K. Biswas, J. Am. Chem. Soc. **142**, 15595 (2020).
[52] M. V. Kovalenko, L. Protesescu, and M. I. Bodnarchuk, Science **358**, 745 (2017).
[53] H. Jin, E. Debroye, M. Keshavarz, I. G. Scheblykin, M. B. J. Roeffaers, J. Hofkens, and J. A. Steele, Mater. Horiz. **7**, 397 (2020).
[54] W. J. Yin, T. Shi, and Y. Yan, J. Phys. Chem. C **119**, 5253 (2015).
[55] W. Ming, H. Shi, and M. H. Du, J. Mater. Chem. A **4**, 13852 (2016).
[56] J. L. Martins and A. Zunger, Phys. Rev. B **30**, 6217(R) (1984).
[57] J. Yang, P. Zhang, and S.-H. Wei, J. Phys. Chem. Lett. **9**, 31 (2018).